Available online at www.sciencedirect.com
ScienceDirect
Journal of Power Sources 168 (2007) 31–39
JOURNAL OF POWER SOURCES
www.elsevier.com/locate/jpowsour

Modeling of the charge acceptance of lead–acid batteries

M. Thele [a,*], J. Schiffer [a], E. Karden [b], E. Surewaard [b], D.U. Sauer [a]

[a] *Electrochemical Energy Conversion and Storage Systems Group, Institute for Power Electronics and Electrical Drives (ISEA), RWTH Aachen University, Jaegerstrasse 17-19, D-52066 Aachen, Germany*
[b] *Ford Research Center Aachen, Aachen, Germany*

Received 13 October 2006; received in revised form 18 November 2006; accepted 21 November 2006
Available online 3 January 2007

Abstract

This paper presents a model for flooded and VRLA batteries that is parameterized by impedance spectroscopy and includes the overcharging effects to allow charge-acceptance simulations (e.g. for regenerative-braking drive-cycle profiles). The full dynamic behavior and the short-term charge/discharge history is taken into account. This is achieved by a detailed modeling of the sulfate crystal growth and modeling of the internal gas recombination cycle. The model is applicable in the full realistic temperature and current range of automotive applications.

For model validation, several load profiles (covering the dynamics and the current range appearing in electrically assisted or hybrid cars) are examined and the charge-acceptance limiting effects are elaborately discussed. The validation measurements have been performed for different types of lead–acid batteries (flooded and VRLA). The model is therefore an important tool for the development of automotive power nets, but it also allows to analyze different charging strategies and energy gains which can be achieved during regenerative-braking.

Keywords: Frequency domain; Model; Overcharging; Charge acceptance; Lead–acid; VRLA

1. Introduction

Insufficient charge acceptance is one of the major concerns for lead–acid batteries in applications with limited charging times or a need for a high dynamic charge acceptance. Many authors have reported these battery problems and they were recently summed up in [20]. Most battery models fail to simulate charging processes at high rates or close to full charging accurately. Therefore, this paper focuses on the depletion of Pb^{2+} ions as the primary limiting process during dynamic charging. An adequate modeling approach of this effect is proposed (Section 4) which supplements a comprehensive impedance-based model for lead–acid batteries, which we have presented earlier [8,24,25].

Since the charge acceptance occurs as part of the general operation of a battery, a full model is necessary to describe processes such as charge-transfer reactions, gassing reactions and electrolyte-transport processes. Short descriptions with corresponding references to the theory and the model topologies are given in Section 3.2.

2. Depletion of Pb^{2+} ions during overcharge

This effect is modeled by submodels (for each electrode) in the latest model version [25] and has been identified to be the main limiting process during charging at high current rates or high states of charge under dynamic operation. The decrease of the Pb^{2+} ion concentration is caused by the generation of Pb and PbO_2 from Pb^{2+} ions in the negative and the positive electrode, respectively. A liquid phase dissolution/crystallization process is assumed. The dissolution process of the $PbSO_4$ crystals limits Pb^{2+} ion delivery. This causes a significant overvoltage and the charge acceptance of the battery is limited if maximum charging voltage limits are used, which is in fact the case in most applications. During operation at moderate current rates and low states of charge, the dissolution rate of $PbSO_4$ crystals is high and, consequently, it is not recognized as a limiting process. A theory for homogeneous nucleation and the subsequent growth of $PbSO_4$ crystals has been proposed by Kappus [13] and has been

* Corresponding author. Tel.: +49 241 8096945; fax: +49 241 8092203.
E-mail address: batteries@isea.rwth-aachen.de (M. Thele).

0378-7753/$ – see front matter © 2006 Elsevier B.V. All rights reserved.
doi:10.1016/j.jpowsour.2006.11.088

developed further for simulation models by Sauer [19]. This algorithm is part of the model presented in this paper.

The processes of crystal solution and the transport of Pb^{2+} ions have also been identified by other researchers as important charge-acceptance limiting processes. Petkova and Pavlov [17] investigated the influences of different charge modes on the negative electrode and considers thereby that lower acid concentrations inside the pores lead to a higher solubility of the $PbSO_4$ crystals. Also for this reason, a third charging step with moderate constant current rate is recommended by Petkova for fully charging of the NAM. Takehara [22] imputes the limited charge acceptance of the negative electrode to the limited mass transfer of Pb^{2+} ions and a consequential depletion. However, charging of the positive electrode is reported to be mainly limited by charge transfer. This is inline with our observations which are discussed in Section 6. The modeling approach of the Pb^{2+} ions depletion is presented in Section 4.

2.1. Process of "Hardening Crystals"

A further process needs to be recognized which becomes obvious during extended experimental tests with lead–acid batteries. If a battery undergoes shallow cycles around a fixed state of charge, the charge acceptance increases with increased cycling time. This leads to the assumption that the newly formed sulfate crystals can be dissolved during charging easier than sulfate crystals that have been formed earlier. To cope with this effect, an additional modeling approach of "Hardening Crystals" has been introduced. Hereby, crystals that have been formed recently have a higher dissolution rate than older crystals. Fig. 1 illustrates the effect by considering charging and discharging steps with rest periods in between.

The duration of each step is 10 s and the discharging current is doubled after eight repetitions (-7, -14, $-28I_{20}$). The charging steps are unlimited in current rate but voltage limited at 2.45 V. Hence, the controlled current during charging can be evaluated as a measure of charge acceptance. Having the discharge current doubled (e.g. from $-14I_{20}$ to $-28I_{20}$, Fig. 1 (right hand)), the accepted current rate during charging increases stepwise in each case. Neither a significant change of SOC (which is smaller than 0.4% of C_N) nor a significantly pronounced acid concentration gradient (the open-circuit voltages are nearly the same after each rest period, Fig. 1 (right hand)) can explain the observed behavior. Moreover, the observations cannot be imputed to significantly more discharged double-layer capacities since the measured capacity values are too small (or the measured overpotentials after rest periods should differ much more, respectively). Consequently, the solubility of the $PbSO_4$ crystals after the different discharging periods seems to vary.

Equal observations are published numerously by Yamaguchi and co-workers [24,16]. By Electro-Chemical Atomic Force Microscopy technique (EC-AFM) he observed a changing morphology of the crystal distribution in a range of minutes during open-circuit standing. The resulting influences on the charge acceptance have been investigated and proven particularly for the negative electrode. He also proposed a model which is quite similar to the "Hardening Crystals" modeling approach which is described in detail in Section 4.2.

3. Lead–acid battery modeling

3.1. General information on electrical-circuit models

As batteries are non-linear and highly dependent on divers parameters like temperature, state of charge (SOC) and short-term history [6], the implementation of battery models is very difficult and a simple modeling with high precision is consequently nearly impossible. However, fast computing and small parameterization effort are mainly needed. A good compromise can be achieved by employing equivalent electrical-circuit models which allow high computing speed and the representation of the physico-chemical processes by electrical components as inductors, capacitors and resistors.

Such modeling approaches have been presented recently by several groups. Barsoukov et al. and Buller [2,7] demonstrated the applicability of this approach to several battery technologies by using non-linear components. Hejabi et al. [12] models the kinetic behavior of the positive lead acid electrode. For

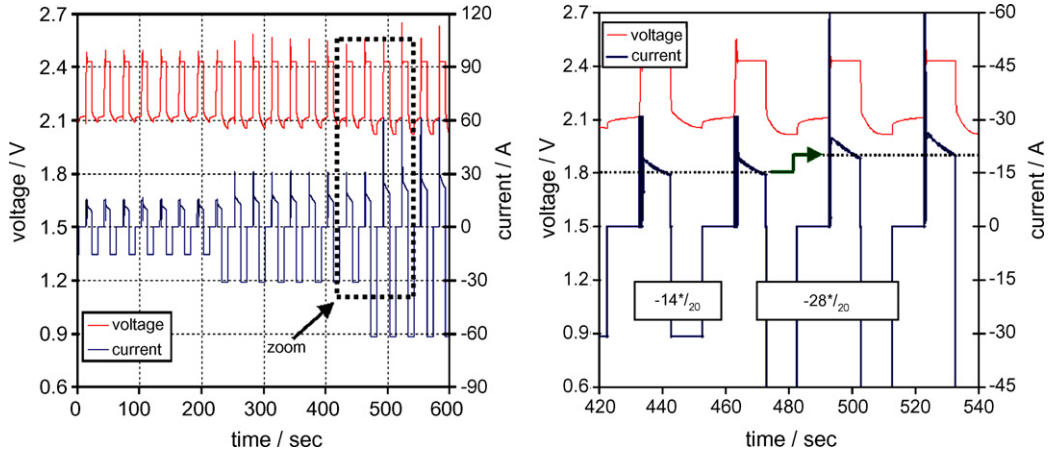

Fig. 1. Illustration of voltage and current data during alternating current steps (recorded at 25 °C and 90% SOC); stepwise increase of charge acceptance becomes obvious after the discharge current is doubled.

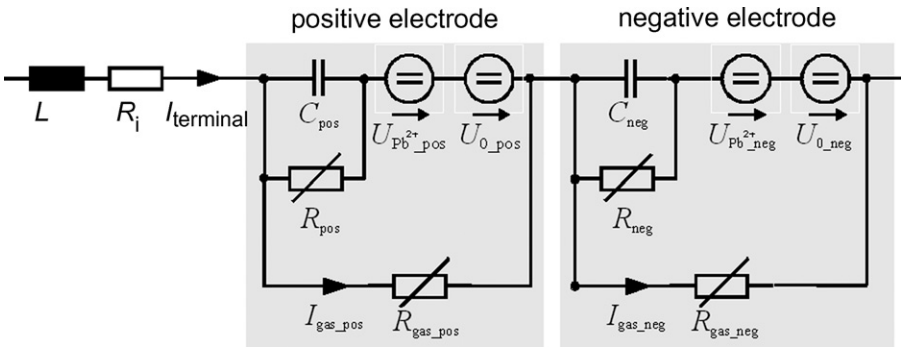

Fig. 2. The complete battery model topology considering physico-chemical processes with electrical elements (Table 1).

state of charge diagnosis of lead–acid batteries, the approach is employed by Salkind et al. and Abolhassani et al. [21,1]. Formerly, Mauracher and Karden [15] also proved the possibilities of this approach using a highly non-linear model whereby the validity range was limited to the range of 10–90% SOC and the charging current was limited to small rates.

Electrochemical impedance spectroscopy [14] can be employed adequately for parameterization of these electric-circuit models. Small-signal excitations and the evaluation of the system's response enables accurate investigations at nearly any working point [8] at which the non-linearity of the system is taken into account. A highly precise measurement hardware ("EISmeter") has been developed therefore at our institute which performs impedance spectroscopy in galvanostatic mode [5].

3.2. Overview of the complete model structure

The structure of the battery model is given in Fig. 2. The physico-chemical processes are considered by electrical elements and are specified in Table 1. The following sections briefly give descriptions why these effects influence charge acceptance and inform about the modeling approaches. However, the focus lies on the voltage sources $U_{Pb^{2+}pos}$ and $U_{Pb^{2+}neg}$ which represent the resulting overpotentials when a depletion of Pb^{2+} ions occurs (Section 4).

3.2.1. Charge-transfer processes

This process is characterized by a highly non-linear relationship ("Butler–Volmer") between the charge-transfer (or "exchange") current density and the corresponding overpotential [6]. Particularly at high states of charge, the overpotential can increase significantly during charging. The charging current has to be reduced when a defined voltage limit is reached. Consequently, the charge acceptance is limited. These processes can be measured adequately by impedance methods and are employed as non-linear resistors in the electrical-circuit model in parallel connection to the double-layer capacitors [8,25].

Table 1
Specification of electrical elements illustrated in Fig. 2

Notation	Meaning
L (H)	Inductance
R_i (Ω)	Ohmic resistance
C_{pos}, C_{neg} (F)	Double-layer capacitance
R_{pos}, R_{neg} (Ω)	Non-linear charge-transfer resistance
U_0 (pos/neg) (V)	Electrode potential calculated by electrolyte-transport model
R_{gas} (pos/neg) (Ω)	Non-linear gassing behavior
$U_{Pb^{2+}}$ (pos/neg) (V)	Overpotential caused by Pb^{2+} ion depletion

3.2.2. Gassing reactions

The charge acceptance is limited by the secondary reactions as they can take a main part of the terminal current at high electrode potentials. These reactions [3,4,11] are employed as submodels which are replaceable for flooded or AGM cells. Oxygen evolution at the positive, hydrogen evolution at the negative and oxygen reduction at the negative electrode (for AGM cells) are considered. The models are parameterized by applying different constant currents at fully charged state of the battery and evaluation of the resulting electrode potentials [25].

3.2.3. Electrolyte-transport

If strong variations of the acid concentrations gradients occur (e.g. during intensive charging with high Ah throughputs), the electrode potentials can be significantly increased. Hence, the difference to a defined upper voltage limit is decreased and the overpotentials for the charging reactions are more restricted. This leads to a reduction of charge acceptance. A basic electrolyte-transport model is employed therefore which describes the generation and the transport of sulfuric acid inside and between the porous electrodes [24]. A spatial resolution of three volume elements has been chosen to allow high computation speed with sufficient precision in predicting the electrical battery performance. A similar approach has already been used by Ekdunge [9].

4. Modeling the depletion of Pb^{2+} ions

According to basic electrochemical laws, overpotentials occur (Eqs. (1) and (2)) if the ratio of the actual ion concentration c and the equilibrium concentration c_s (as a function of temperature and acid concentration, Fig. 3) deviates.

An ion depletion and hence an actual ion concentration which is lower than the equilibrium concentration results in a positive overvoltage at positive electrode and a negative overvoltage at

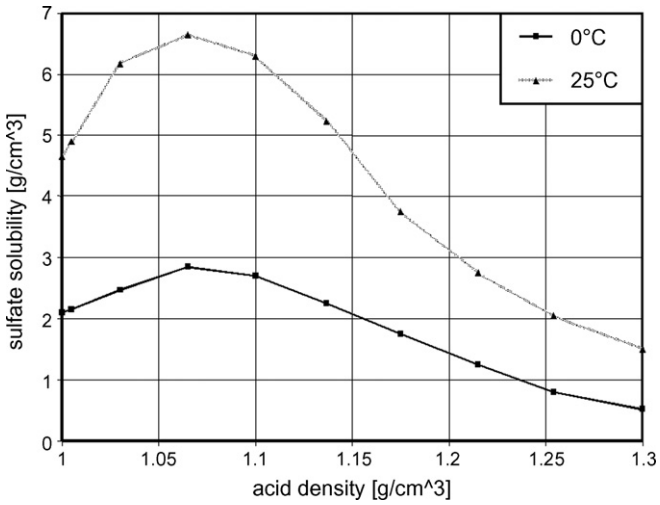

Fig. 3. Sulfate solubility as a function of temperature and acid concentration.

the negative electrode. As a consequence, the cell voltage is increasing. This relation holds for any type of dissolved ions.

positive electrode:

$$U_{\mathrm{Pb^{2+}pos}} = -\frac{RT}{nF}\ln\left(\frac{c}{c_\mathrm{s}}\right) \tag{1}$$

negative electrode:

$$U_{\mathrm{Pb^{2+}neg}} = \frac{RT}{nF}\ln\left(\frac{c}{c_\mathrm{s}}\right) \tag{2}$$

R corresponds to the gas constant, F to the Faraday constant, T to the temperature (K) and $n = 2$ to the valence of Pb^{2+} ions. Fig. 4 depicts that the battery voltage is significantly influenced by this effect (illustrated during alternating charging and discharging pulses). Although the charging current is simply doubled from $2I_{20}$ (4.4 A) to $4I_{20}$ (8.8 A) for a few seconds, the overvoltage during charging raises disproportionately high (from ~40 to ~230 mV).

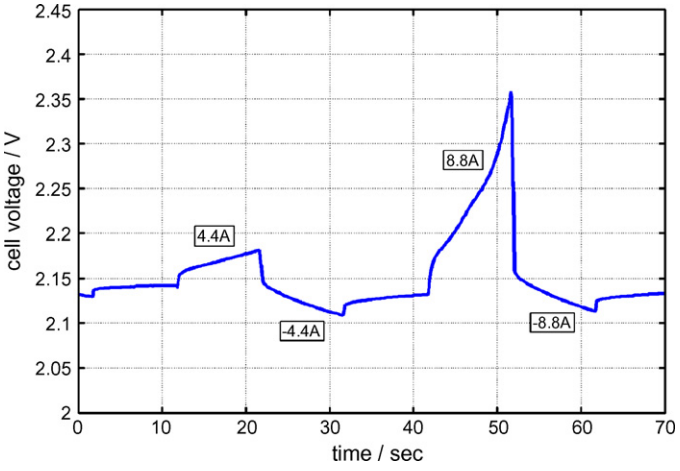

Fig. 4. Typical beginning of overcharging effects at 8.8 A ($4I_{20}$) due to Pb^{2+} ion depletion, voltage measured during alternating charging and discharging steps at 90% SOC and 25 °C.

The change of the actual ion concentration c is defined by the balance of the rate density of the generated or absorbed Pb^{2+} ions q (due to the main-reaction current) and the rate density of the ions s arising from crystallization or dissolution of $PbSO_4$ crystals (Eqs. (3) and (4) with I as a current density).

$$\dot{c} = q - s \tag{3}$$

$$q = \frac{I}{2F} \tag{4}$$

4.1. Solubility of $PbSO_4$ crystals

The limitation of the dissolution process is assumed to be the main cause for Pb^{2+} depletion. Apart from acid concentration and temperature, the solubility dependents on the total $PbSO_4$ surface which again is a function of the absolute $PbSO_4$ volume $V_{\mathrm{PbSO_4}}$ (SOC = 100% ⇒ $V_{\mathrm{PbSo_4}} = 0$, SOC = 0% ⇒ $V_{\mathrm{PbSo_4}} = V^{\max}_{\mathrm{PbSo_4}}$) and the crystal-size distribution. The employed algorithm for calculation of $V_{\mathrm{PbSO_4}}$ and the crystal size distribution is not described here but can be found in [25].

$$s = 10(c - c_\mathrm{s})V_{\mathrm{PbSO_4}}\frac{D}{\sigma^2} = 10(c - c_\mathrm{s})V_{\mathrm{PbSO_4}}D_\mathrm{eff} \tag{5}$$

4.2. "Hardening Crystals" approach

As mentioned in Section 2, the charge acceptance can increase significantly during shallow cycles even though the state of charge is changed very slightly. Fig. 5 serves as a simplified illustration of the implemented "Hardening Crystals" approach: a $PbSO_4$ crystal is characterized by high solubility shortly after discharging (start of time arrow). In case of open-circuit standing without current flow, the hardened part of the crystal (with lower solubility) grows with time (Fig. 5, upper row). When the battery is charged (lower row), two effects are present. The hardened part grows with time and the total volume of the crystal decreases according to the calculation of $V_{\mathrm{PbSO_4}}$ and the dissolution rate s (see Section 4.1).

The model implementation has been implemented by means of a *RC*-element as shown in Fig. 6. According to the model, currents flowing via the resistor are accounted as hardened crystal

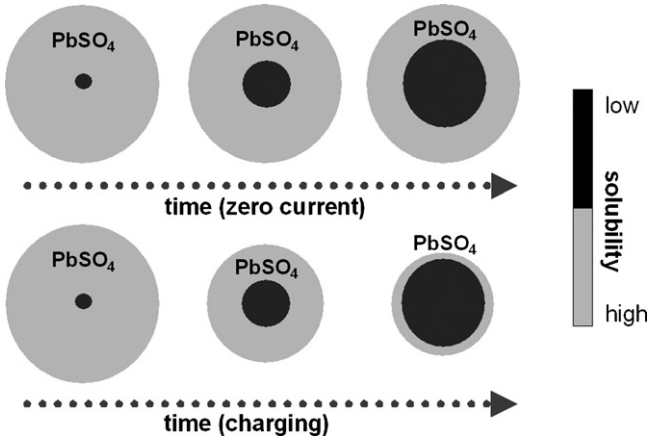

Fig. 5. Simplified illustration of the "Hardening Crystals" approach.

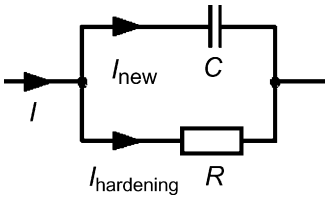

Fig. 6. Calculation of hardening effect in terms of a *RC*-element.

parts ($Q_{hardened}$), the current which is accumulated on the capacitor (Q_{new}) are newly formed crystal parts with high solubility (see Eq. (6)).

The size of the capacitor limits the amount of the sulfate crystals with high solubility. During rest periods (no new sulfate crystals are formed) a transformation from newly formed to hardened crystals takes place by means of a discharge of the capacitor. The parameter $Q_{hardened}$ and Q_{new} are restricted to positive values, discharging currents are expressed by negative values (discharging: $I_{battery} < 0$).

$$Q_{new} = \int \left(-\frac{I_{battery}}{2F} - \frac{\partial Q_{hardened}}{\partial t} \right) dt \quad (6)$$

The time constant $\tau = RC$ determines the hardening speed of the crystals. The variable solubility of the crystals is considered as a modified diffusion constant D_{eff} given by Eq. (7). Thus, two parameters (τ and $k_{hardening}$) have to be determined by measurements. $k_{hardening}$ can be derived from measurements as they have been shown in Fig. 1. For the determination of, long-term measurements are necessary to specify the time dependent process of hardening. Such an experimental procedure is illustrated in Section 5.2 (Fig. 11) whereby equal high rate charging pulses have been applied to the battery in a range of an hour and the accepted amount of charge can be evaluated, respectively.

$$D_{hardening} = (1 + (k_{hardening} n_{new})) D_{eff} \quad (7)$$

It is worth to mention, that this is a mathematical approach to model an experimental observed effect. We chose a modification of the diffusion constant, thus anticipating that the number and size of the crystals is not changing as long as no external charge or discharge current flows. The work of Yamaguchi et al. [26] also allows the assumption, that a recrystallization process takes place in the first minutes after crystals have been formed which leads to a reduction of the number of crystals while their size increases. This in fact results in reduction of the available surface and the surface area also changes the solubility. Therefore, the observed effect can be described either by the change of the crystal surface or by a modification of the diffusion constant. For the modeling of the observed effects this makes no difference.

Table 2
Employed battery samples for model evaluation

Manufacturer	Technology	Nominal capacity	Nominal voltage
JCI (optima)	VRLA/AGM spiral wound	44 Ah	12 V
Varta	Flooded, SLI	60 Ah	12 V

5. Simulation results

Different load profiles were applied to two different battery types and the corresponding parameterized battery models for evaluation. Table 2 depicts the nominal data of the considered battery types. Please note that all above mentioned processes (Sections 3.2 and 4) are considered simultaneously during the simulation.

5.1. VRLA/AGM battery

Fig. 7 depicts a section of a load profile with several discharging and charging steps similar to the data given in Fig. 1. The simulation was performed using a PI-controller during the voltage limited charging periods. Both, the stepwise increase of the charge acceptance after the changed discharge rate (in the range from 1500 to 1550 s ("A")) and the dynamic behavior of the controlled current during the charging steps ("B") were simulated with very good agreement to the measured data. The measurement was carried out at room temperature and 90% state of charge.

5.2. Flooded lead–acid battery

A slightly modified test procedure was employed for the evaluation of the model for the flooded battery. The procedure and absolute values are given in Table 3. Again, alternating steps

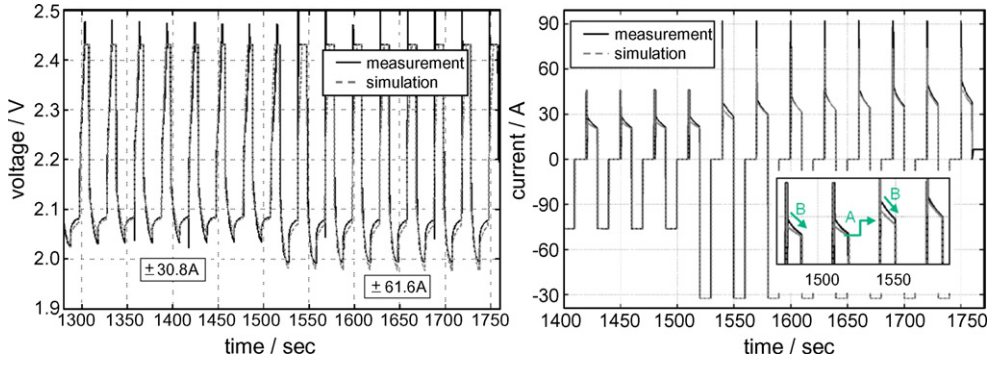

Fig. 7. Simulation and measurement results of the VRLA/AGM battery (90%, *RT*, 44 Ah) with voltage limited charging ($U_{limit} = 2.45$ V); left hand: battery voltage; right hand: terminal current.

Table 3
Applied test procedure

Step	Purpose	Values
1	SOC setting (start at 100% SOC)	$I_{batt} = I_N = 3$ A
2	Rest period	$t_{pause} = 3$ h
3	[Alternating current pulses with 1 s duration each and increasing current rates/charge equalization step] triple repetition	$I_{batt} = -700$ to +90 A; $t_{pulse} = 1$ s; $I_{equalization} = 3$ A
4	[Alternating current pulses with 10 s duration each and increasing current rates/charge equalization step] triple repetition	$I_{batt} = -300$ to +90 A; $t_{pulse} = 10$ s; $I_{equalization} = 3$ A
5	[Alternating current pulses with 100 s duration each and increasing current rates/charge equalization step] triple repetition	$I_{batt} = -90$ to +90 A; $t_{pulse} = 100$ s; $I_{equalization} = 3$ A

with increasing current rates were applied by considering a different step duration of 1, 10 and 100 s. An equalization step (charging) was further introduced to keep the same SOC during the test. To assure reproducibility, all profiles with x s duration were repeated three times.

Measurement and simulation results are depicted in Fig. 8 (10 s pulses) and Fig. 9 (100 s pulses) which were recorded at 90% SOC and 25 °C. Good agreement can be observed again, however slight deviations become obvious in Fig. 8 at 495.5 min and in Fig. 9 at 570 min (635 min, respectively). These errors will be discussed in Section 6.

The state of charge was calculated during the test procedure (given in Table 3) for the measured and the simulated data. Fig. 10 illustrates the results at 90% SOC (left hand) and 70% SOC (right hand). The necessity of a correctly simulated charge acceptance manifests by considering the solid black lines which were calculated according to simulation data without limited charge acceptance. The deviations are smaller at lower SOC since the limited charge acceptance is more pronounced at higher SOC.

To demonstrate further the applicability of the "Hardening Crystals" modeling approach, Fig. 11 focuses on a three times repetition of a charging step (10 s duration) which was applied to a battery in a range of 1 h with equal time periods and discharging steps for SOC equalization in between. Before, the battery had been discharged from 100 to 90% SOC with a subsequent rest period of 3 h. The nominal current of −3 A was applied for both, equalization and discharging to 90% SOC. The battery was a 60 Ah flooded SLI battery (Varta) at 25 °C controlled ambient temperature. The left hand figure illustrates the measured

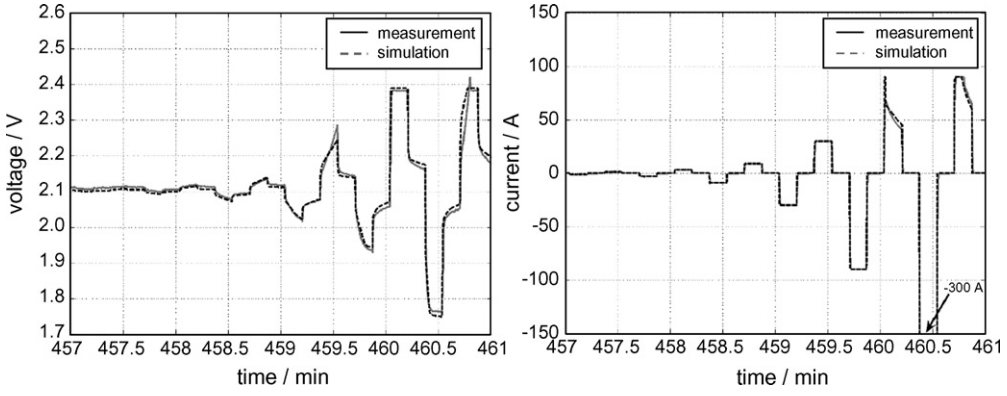

Fig. 8. Single cell measurement and simulation of a VARTA SLI battery (flooded) with $U_N = 12$ V and $C_N = 60$ Ah ($T_{amb} = 25$ °C, SOC = 90%, $U_{max,cell} = 2.4$ V), 10 s pulses.

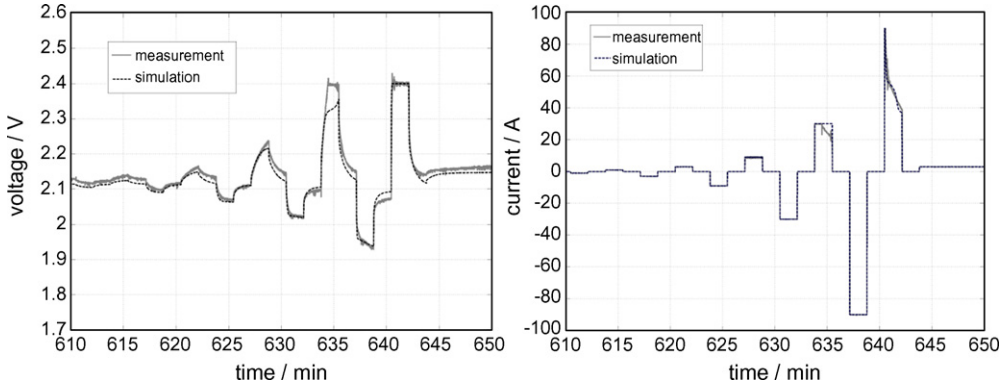

Fig. 9. Single cell measurement and simulation of a VARTA SLI battery (flooded) with $U_N = 12$ V and $C_N = 60$ Ah ($T_{amb} = 25$ °C, SOC = 90%, $U_{max,cell} = 2.4$ V), 100 s pulses.

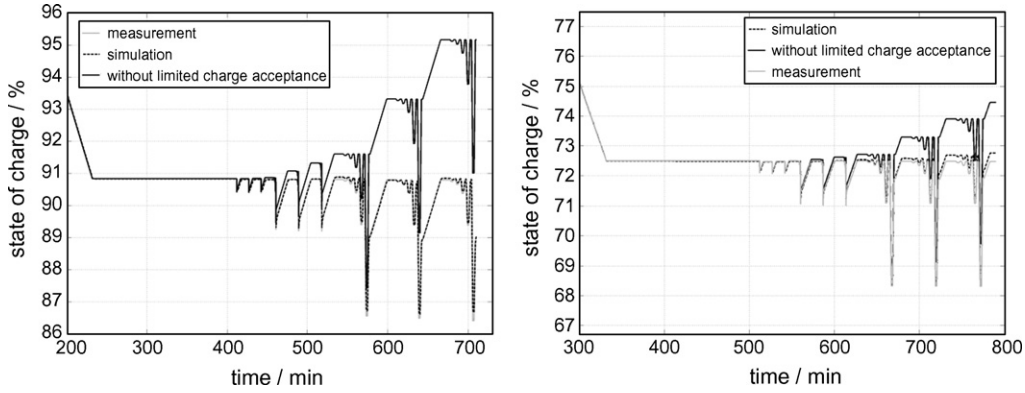

Fig. 10. State of charge during test procedure (Table 3), very good agreement between measured and simulated values when the limited charge acceptance is considered (left hand: test procedure at approx. 90% SOC; right hand: test procedure at approx. 70% SOC).

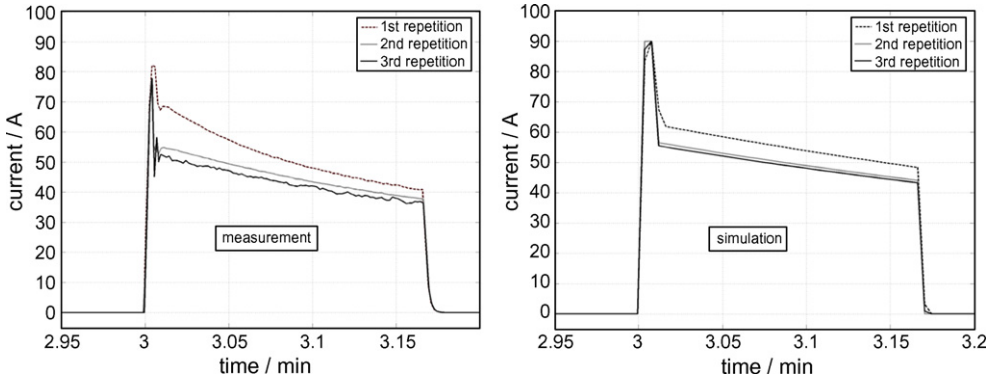

Fig. 11. Measured and simulated battery current during voltage limited (2.4 V) charging steps in a range of 1 h at 25 °C and 90% SOC (Varta flooded SLI battery with $C_N = 60$ Ah and $U_N = 12$ V).

current data, the simulated data which has been obtained by a continuous simulation of the described procedure is given on the right hand. Both, the dynamic behavior (during each step) and the decreasing charge acceptance from repetition to repetition can be represented with quite good agreement.

6. Discussion

6.1. Charge-acceptance limiting effects

As mentioned, various effects are involved during overcharging. If highly dynamic load profiles with very small Ah throughputs are applied at moderately high states of charge, only minor acid concentration gradients have to be expected and the contribution of the side reactions is small (at least in contrast to the terminal current). This applies to the profile depicted in Fig. 8 (10 s pulse duration, 90% SOC) during which the depletion of Pb^{2+} ions and the charge transfer as the main limiting factors of charge acceptance can be estimated consequently. Besides the measured cell voltage, the electrode potentials were recorded as well using a $Hg/Hg_2SO_4/H_2SO_4$ reference electrode. The results are depicted in Fig. 12 as single cross-markers and absolute values. The corresponding current rates are given in Fig. 8 (right hand). A disproportionate

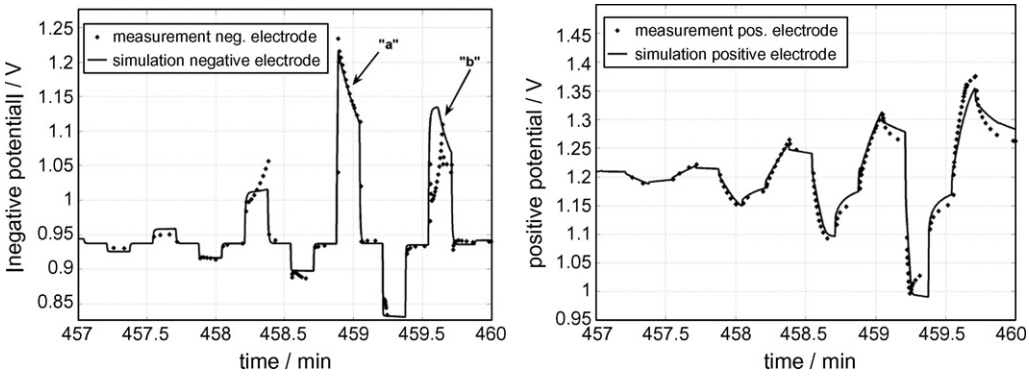

Fig. 12. Electrode potentials according to the results in Fig. 8; depletion effect at negative electrode becomes obvious by a significantly increased potential (“a”).

Table 4
Modified test cycle based on Table 3

Step	Purpose	Values
1	Setting of 90% SOC (start at 100 or 40%, respectively)	$I_{batt} = I_N = \pm 3$ A
2	Different rest periods	$t_{pause} = 0$–24 h
3–5	Same as in Table 3	

increase of the negative overpotential ("a") indicates depletion effects. A noticeably lower negative overpotential during the next charging step ("b") indicates that depletion hardly limits the charge acceptance of the negative electrode this time. The sum of negative and positive potential anyway reaches the defined voltage limit, however without disproportionately high overpotentials compared to the battery current. Hence, the charge acceptance is rather limited by charge-transfer processes. This behavior can be simulated by the presented battery model with the "Hardening Crystals" approach included (solid lines, Fig. 12).

In the case of depletion effects, the voltage increases significantly as illustrated. If the battery model reaches the point of depletion a little earlier or with a small delay compared to the measurement, the measured and simulated voltage can differ significantly. This is mainly the cause for the deviations mentioned in Section 5.2. However, the behavior of the controlled current during voltage limited charging-events could be simulated with less deviations.

6.2. Further impacts on charge acceptance

The influences of state of charge (Section 4.1) and the influences of the short-term history (Section 4.2) on the charge acceptance have been discussed and appropriate models have been proposed. However, the crystals morphology (or solubility, respectively) is influenced further by the long-term history. Modified test cycles based on Table 3 were applied with divers conditioning of the battery at the beginning (Table 4). Both, the SOC setting (step 1, by charging or discharging) and the rest periods in between (step 2) were varied. The test cycle (steps 1–5) was therefore repeated seven times. The current rates for SOC setting corresponded to the nominal current (±3 A).

As a measure for charge acceptance, one charging pulse with 10 s duration (during step 4) was selected with a current rate that assures to achieve the voltage limit (controlled charging current) and depletion effects were detected. Since the profiles were repeated three times ("triple repetition"), three values could be received during each of the seven test cycles. The data evaluation (Fig. 13) illustrates a decreased charge acceptance with increased rest duration which is similar whether the SOC has been set by charging ("after charge") or by discharging ("after dch"). The modeling of this effect based on the "Hardening Crystals" concept is possible. However, the absolute value of charged Ahs differs by approximately factor 2 when the procedure of SOC setting is changed. To find a comprehensive modeling approach, further measurements are planned for the near future.

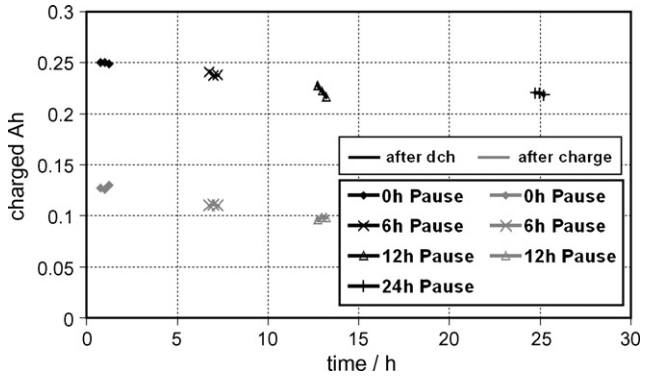

Fig. 13. Charged Ahs during voltage limited charging steps (10 s pulses) by using modified test cycles (see Table 4); Note the different behavior when the initial SOC is adjusted by charging ("after charge") or by discharging ("after dch"); battery under test: Varta flooded SLI battery with $C_N = 60$ Ah and $U_N = 12$ V (90% SOC, 50 °C).

7. Conclusions and summary

A model for lead–acid batteries which includes the modeling of overcharging effects has been presented. Both, charge-acceptance limiting effects have been discussed and adequate modeling approaches have been illustrated. The depletion of Pb^{2+} ions has been identified as the main limiting effect during dynamic charging and a comprehensive modeling approach has been proposed and evaluated by measurements. The approach considers the full dynamic behavior and the short-term charge/discharge history of the battery ("Hardening Crystals" modeling approach).

The complete battery model allows for charge-acceptance tests which are a prerequisite for the development of complex electrical systems such as vehicles with regenerative-braking. The model is applicable in the full realistic temperature and current range of automotive applications and can be used for flooded and VRLA batteries since the gassing models for both technologies are replaceable.

References

[1] N. Abolhassani, N. Gharib, H. Moqtaderi, M. Amin, F. Torabi, A. Mosahebi, M. Hejabi, J. Power Sources 158 (2006) 932–935.
[2] E. Barsoukov, J.H. Kim, C.O. Yoon, H. Lee, J. Power Sources 83 (1999) 61–70.
[3] D. Berndt, J. Power Sources 100 (2001) 29–46.
[4] D. Berndt, Maintenance Free Batteries, third ed., Research Studies Pr, ISBN 0-863-80279-6.
[5] H. Blanke, O. Bohlen, S. Buller, R.W. De Doncker, B. Fricke, A. Hammouche, D. Linzen, M. Thele, D.U. Sauer, J. Power Sources 144 (2005) 418–425.
[6] H. Bode, Lead–acid Batteries, John Willey & Sons, New York, 1977, ISBN 0-471-08455-7.
[7] S. Buller, Impedance-based simulation models for energy storage devices in advanced automotive power systems, PhD Thesis, RWTH Aachen University, ISBN 3-8322-1225-6, 2002.
[8] S. Buller, M. Thele, E. Karden, R.W. De Doncker, J. Power Sources 113 (2003) 422–430.
[9] P. Ekdunge, J. Power Sources 46 (1993) 251–262.
[11] A. Hammouche, M. Thele, D.U. Sauer, J. Power Sources 158 (2006) 987–990.
[12] M. Hejabi, A. Oweisi, N. Gharib, J. Power Sources 158 (2006) 944–948.

[13] W. Kappus, Electrochim. Acta 28 (1983) 1529.
[14] J.R. Macdonald (Ed.), Impedance Spectroscopy, Emphasizing Solid Materials and Systems, John Willey & Sons, New York, 1987, ISBN 0-471-83122-0.
[15] P. Mauracher, E. Karden, J. Power Sources 67 (1997) 69–84.
[16] Y. Nakayama, S. Takahashi, K. Hirakawa, Y. Yamaguchi, J. Power Sources 125 (2004) 135–140.
[17] G. Petkova, D. Pavlov, J. Power Sources 113 (2003) 355–362.
[19] D.U. Sauer, Optimierung des Einsatzes von Blei-Säure-Akkumulatoren in PV-Hybrid-Systemen unter spezieller Berücksichtigung der Batterieal-terung, PhD Thesis, University of Ulm, 2003.
[20] D.U. Sauer, et al., J. Power Sources 168 (2007) 22–30.
[21] A.J. Salkind, P. Singh, A. Cannone, T. Atwater, X. Wang, D. Reisner, J. Power Sources 116 (2003) 174–184.
[22] Z. Takehara, J. Power Sources 85 (2000) 29–37.
[24] M. Thele, S. Buller, D.U. Sauer, R.W. De Doncker, E. Karden, J. Power Sources 144 (2005) 461–466.
[25] M. Thele, E. Karden, E. Surewaard, D.U. Sauer, J. Power Sources 158 (2006) 953–963.
[26] Y. Yamaguchi, M. Shiota, M. Hosokawa, Y. Nakayama, N. Hirai, S. Hara, J. Power Sources 102 (2001) 155–161.